

RESEARCH ARTICLE | OCTOBER 29 2024

# TE-polarized leaky-wave beam launchers: Generation of Bessel and Bessel–Gauss beams

E. Negri ; W. Fuscaldo ; D. González-Ovejero ; P. Burghignoli ; A. Galli 

 Check for updates

*Appl. Phys. Lett.* 125, 181703 (2024)

<https://doi.org/10.1063/5.0234371>



## Articles You May Be Interested In

Microwave generation of X-waves by means of a planar leaky-wave antenna

*Appl. Phys. Lett.* (October 2018)

Multimode interference-based highly sensitive strain sensor by illuminating with a Bessel-Gauss beam

*AIP Conf. Proc.* (October 2020)

High-bandwidth terahertz radiation from ponderomotively accelerated carriers using Bessel–Gauss femtosecond pulses

*Appl. Phys. Lett.* (February 2005)



Applied Physics Letters

# Special Topics Open for Submissions

[Learn More](#)



# TE-polarized leaky-wave beam launchers: Generation of Bessel and Bessel–Gauss beams

Cite as: Appl. Phys. Lett. **125**, 181703 (2024); doi: [10.1063/5.0234371](https://doi.org/10.1063/5.0234371)

Submitted: 21 August 2024 · Accepted: 16 October 2024 ·

Published Online: 29 October 2024








View Online



Export Citation



CrossMark

E. Negri,<sup>1,2,a)</sup>  W. Fuscaldo,<sup>2</sup>  D. González-Ovejero,<sup>3</sup>  P. Burghignoli,<sup>1</sup>  and A. Galli<sup>1</sup> 

## AFFILIATIONS

<sup>1</sup>Department of Information Engineering, Electronics and Telecommunications, Sapienza University of Rome, 00184 Rome, Italy

<sup>2</sup>Istituto per la Microelettronica e Microsistemi, Consiglio Nazionale delle Ricerche, 00133 Rome, Italy

<sup>3</sup>University Rennes, CNRS, Institut d'Électronique et des Technologies du numéRique (IETR), UMR 6164, 35000 Rennes, France

<sup>a)</sup> Author to whom correspondence should be addressed: [edoardo.negri@uniroma1.it](mailto:edoardo.negri@uniroma1.it)

## ABSTRACT

The generation of focused beams in the millimeter- and submillimeter-wave ranges, with transverse-electric (TE) polarization, is investigated in the radiative near-field region. The desired field distribution is achieved through a leaky-wave beam launcher consisting of a grounded dielectric slab with an annular strip grating on top excited by a circular slot on the bottom ground plane. The latter is fed by a Marié transducer, which converts the input, fundamental TE<sub>10</sub> mode of a standard rectangular waveguide into the higher-order TE<sub>01</sub> mode propagating in the circular waveguide connected to the device. The generation of TE-polarized diffraction-limited Bessel and Bessel–Gauss distributions is achieved by suitably synthesizing the annular strip grating. Simulated results are in excellent agreement with those predicted by leaky-wave analysis providing a proof-of-concept for the generation of TE-polarized Bessel and Bessel–Gauss beams at 300 GHz with a beam size of 1.7 and 1.9 mm up to the nondiffractive range of about 25 and 15 mm from an aperture plane with radius of 12.75 mm, respectively.

© 2024 Author(s). All article content, except where otherwise noted, is licensed under a Creative Commons Attribution-NonCommercial-NoDerivs 4.0 International (CC BY-NC-ND) license (<https://creativecommons.org/licenses/by-nc-nd/4.0/>). <https://doi.org/10.1063/5.0234371>

The generation of focused beams at millimeter and submillimeter waves is of tremendous importance in many practical scenarios, such as near-field communications,<sup>1</sup> wireless power transfer,<sup>2,3</sup> and imaging.<sup>4,5</sup> Among all the possible field distributions, Bessel beams (BBs) have gained much attention due to their diffraction-limited<sup>6</sup> and self-healing<sup>7</sup> properties. For this reason, many technologies have been proposed for the synthesis of BBs from microwaves to submillimeter waves.<sup>8–15</sup>

A planar and cost-effective solution is offered by leaky-wave BB launchers.<sup>16,17</sup> Due to the simple implementation of vertical electric dipoles (VEDs) through coaxial connectors, transverse-magnetic (TM) polarization has been preferred for such devices. However, this kind of excitation scheme is commercially available up to 110 GHz (Ref. 18) and it is fragile and expensive for working frequencies above 40 GHz. Moreover, it has recently been shown that a transverse-electric (TE)-polarized BB is interesting from both a theoretical and a practical viewpoint.<sup>19</sup> In particular, it has been recently shown that magnetic resonance can be used to minimize coupling with the surrounding dielectric objects<sup>19</sup> and, thus, TE-polarized BB launchers could be exploited advantageously as emitters in wireless power-transfer<sup>19–22</sup> and imaging, magnetic resonance<sup>23</sup> scenarios thanks to a focusing,

nondiffractive, vertical component of the magnetic field. For these reasons, at microwave frequencies, TE-polarized BBs were first generated through resonant BB launchers,<sup>19–21</sup> showing, nevertheless, limited bandwidth and maximum nondiffractive distances.

This Letter presents an original TE-polarized wideband BB launcher<sup>16</sup> with a realistic feeding network working around 300 GHz. The device is constituted by a grounded dielectric slab (GDS) with an annular metal strip grating on top and it is excited by a circular slot etched on the ground plane. This structure is hereafter referred to as *radially periodic leaky-wave beam launcher* and is sketched in Fig. 1 along with a qualitative field distribution. The circular slot is fed by a circular waveguide (CW) where only the higher-order TE<sub>01</sub> mode propagates. This is achieved through a Marié transducer [see Fig. 2(a)],<sup>25,26</sup> which is suitably matched to a standard WR3 rectangular-waveguide input using the semi-analytical approach in Ref. 24. Moreover, by properly tapering the aperture-field distribution, a leaky-wave Bessel–Gauss beam (BGB)<sup>27</sup> has been obtained. In this manner, the first generation of a BGB both at submillimeter-wave frequencies and with TE polarization is demonstrated.

We start here from discussing the design of a TE-polarized BB launcher, thus based on a nontapered aperture distribution, and the

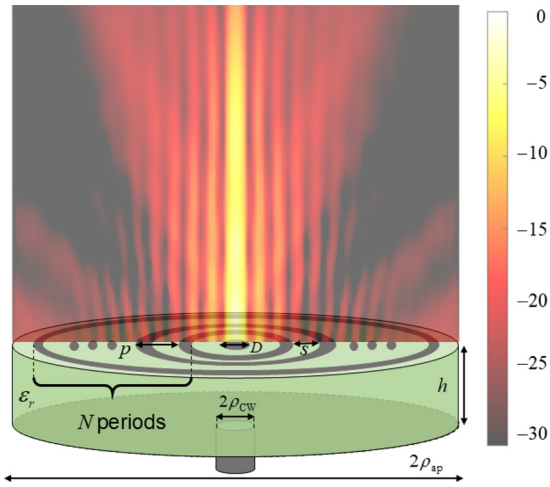


**FIG. 1.** Representation of a TE-polarized radially periodic leaky-wave launcher excited by a CW through a slot on the ground plane. The near-field  $|H_z|$  distribution, normalized with respect to its maximum, is qualitatively reported through a dB color-map for the proposed TE BB launcher.

realization of its feeding network. An azimuthally symmetric TE-polarized Bessel beam requires a vertical-magnetic dipole (VMD) excitation. At microwave and submillimeter-wave frequencies, practical realizations of VMDs are not as simple as for VEDs.<sup>20</sup> The typical VMD implementation is indeed usually constituted by loop antennas or coils<sup>19,21</sup> but their feeding point breaks the azimuthal symmetry of the device and excites both TE and TM components.<sup>17</sup> An alternative solution is to synthesize a realistic counterpart of a radially directed magnetic current.<sup>28</sup> At microwave frequencies, the latter can be achieved through a radial slot array on the ground plane fed through microstrip lines.<sup>20</sup> In order to avoid the technological challenges posed by the excitation of multiple slots at millimeter and submillimeter waves, we here replace the radial slot array with a simple circular slot on the ground plane fed through a CW that propagates only the higher-order TE<sub>01</sub> mode.<sup>29</sup>

An *ad hoc* mode converter has been implemented to achieve the TE<sub>01</sub> mode in the CW from a standard WR3 working in the

**TABLE I.** Design parameters of the proposed Marié transducer in millimeters.

$a_{WR3}$	$a_1$	$a_2$	$a_3$	$a_4$	$\rho_{CW}$	$L_{CW}$
0.8636	0.6521	0.2156	0.2919	1.3384	0.65	0.8152
$b_{WR3}$	$b_1$	$b_2$	$b_3$	$b_4$	$g_1$	$g_2$
0.4318	0.2630	1.3069	1.3384	0.2919	0.0216	0.054
$L_1$	$L_2$	$L_3$	$L_4$	$L_5$	$d_1$	$d_2$
1.2954	3.2606	0.6521	1.6303	1.6303	0.25	0.7325

220–330 GHz range, which is the typical antenna excitation in the upper millimeter- and submillimeter-wave regime.<sup>30</sup> In particular, a Marié transducer with an additional matching section is considered. From a practical viewpoint, the latter cannot be realized at submillimeter-wave frequencies through a 3D printer since the surface roughness limits its application beyond the W-band.<sup>31,32</sup> On the other hand, the fabrication of a Marié transducer using only computer numerical control (CNC) milling is a challenging task as it requires a 5-axis machine and multiple parts. For this reason, the simpler implementation of the device could rely on a combination of CNC milling with platelet fabrication for the complex cross sections; the latter technique has been proven effective at frequencies as high as 560 GHz.<sup>33</sup> As concerns, instead, the theoretical viewpoint, the working principle of the mode converter is explained in Ref. 26: the TE<sub>10</sub> mode coming from the feeding WR3 is totally converted into the TE<sub>01</sub> CW mode since it is the first mode supporting the symmetries and field structure of the desired radially directed magnetic current. Propagation of the TE<sub>41</sub> mode, which is the next higher-order mode after the TE<sub>01</sub>, is prevented by properly selecting the waveguide radius  $\rho_{CW}$ .

According to these design rules, a converter with the geometrical parameters given in Table I is designed and simulated in CST Microwave Studio with an input WR3 port and an output CW one. As can be inferred by the scattering parameters in Fig. 2(b), the converter properly works in the 290–330 GHz frequency range, achieving nearly unitary power transmission from the fundamental TE<sub>10</sub> mode at the input rectangular port to the desired TE<sub>01</sub> mode at the output circular

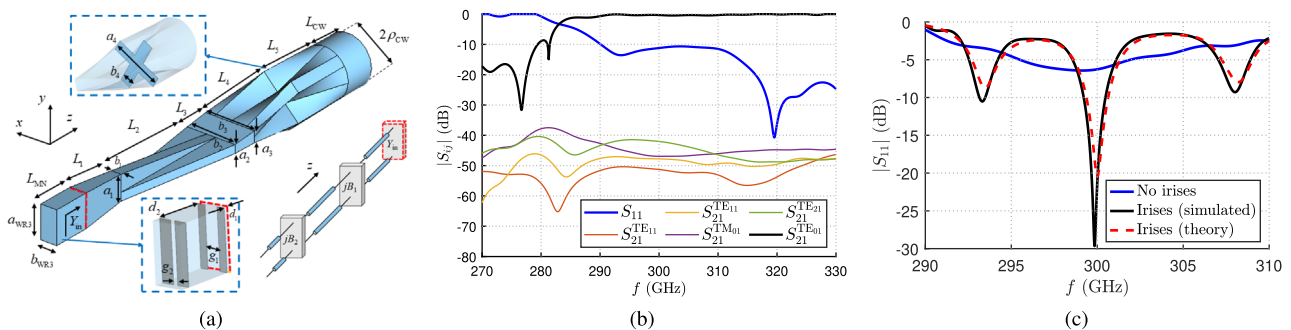


**FIG. 2.** (a) Schematic view of the proposed Marié transducer with its geometrical parameters. The initial WR3 section of length  $L_{MN}$  works as a simple matching network of the device through a pair of capacitive irises and its equivalent transmission-line model is reported on the right.<sup>17</sup> (b) Magnitude in dB of the S-parameters when the Marié transducer is considered as a two-port network with a WR3 input port and a CW output port. (c) Magnitude in dB of  $S_{11}$  when the Marié transducer is connected to the BB launcher with (black solid line) and without (blue solid line) matching irises. The red dashed line represents the theoretical prediction of  $S_{11}$  thanks to a circuital representation of the matching network.<sup>24</sup>

port. It is worth pointing out that, as desired, all the modes with lower cutoff frequencies with respect to the  $TE_{01}$  mode are suppressed, as their  $S_{21}$  parameters have magnitude lower than  $-40$  dB. Moreover, as can be seen from  $S_{11}$ , the device impedance bandwidth covers the desired bandwidth with a matched output port. However, when the Marié transducer is implemented as a feeder for the TE-polarized BB launcher, the load impedance is different and a matching network is needed [see the  $S_{11}$  blue curve in Fig. 2(c)]. The latter can be implemented through two capacitive irises in the first feeder section, which has a length  $L_{MN} = \lambda_0$  (with  $\lambda_0$  being the free-space wavelength at the working frequency  $f_0 = 300$  GHz) and lateral dimensions  $a_{WR3}$  and  $b_{WR3}$ .

The matching network is designed by following the approach in Ref. 24. The method only requires a single full-wave simulation of the mode converter (without the matching irises) exciting the BB launcher to retrieve the input impedance  $Y_{in}$  at the reference plane marked by the dashed red line in Fig. 2(a). The latter is exploited as the load for a matching-network transmission-line equivalent model to represent the radiating device. In this manner, the design parameters of the capacitive irises, namely, the gap dimensions  $g_1$  and  $g_2$ , and their distance with respect to the reference plane,  $d_1$ , and to each other,  $d_2$ , can be optimized through a fully numerical technique based on analytical, closed formulas [see Fig. 2(a)]. In particular, the waveguide discontinuities are represented as shunt elements with equivalent susceptances  $B_1$  and  $B_2$  whose formulas, reported in Ref. 34, are functions of  $g_1$  and  $g_2$ . An ultra-fast optimization procedure can thus be carried out to obtain the design parameters of the matching network by exploiting transmission-line theory.<sup>24</sup> At  $f_0 = 300$  GHz, the procedure provides the dimensions of gaps and the distances of the two irises, viz.,  $g_1$ ,  $g_2$ ,  $d_1$ , and  $d_2$  shown in the inset in Fig. 2(a) and reported in Table I. After this matching procedure, the magnitude of the reflection coefficient is significantly reduced, as shown by the red dashed line in Fig. 2(c). The effectiveness of the equivalent transmission line is corroborated by the full-wave simulation of the entire BB launcher (whose design is discussed below) represented with the black solid line  $S_{11}$  in Fig. 2(c).

The leaky-wave analysis and the design of a TE-polarized BB launcher requires the evaluation of dispersion curves of the relevant leaky radial wavenumber.<sup>17,20</sup> The device is based here on an annular metal strip grating printed on top of a GDS. Owing to its azimuthal symmetry, the dispersion curve of the structure can efficiently be

evaluated through the analysis of its linearized 1D counterpart.<sup>16</sup> Different methods are known for the evaluation of the leaky wavenumber, referred to as  $k_p = \beta - j\alpha$ , with  $\beta$  and  $\alpha$  being the leaky phase and attenuation constants.<sup>35–37</sup> In this work, by enforcing a TE-polarized propagation mode in a 1D metal strip grating configuration simulated on CST Microwave Studio, the  $\beta$  and  $\alpha$  dispersion curves have been extrapolated by the unit-cell  $T$  matrix. The latter is evaluated through the  $T$ -matrices of truncated structures with  $N = 6$  and  $N = 7$  periods on the full-wave solver (a similar approach has been shown in Ref. 38).

The dispersion-analysis results are reported in Fig. 3(a) through the dispersion curves of the phase and attenuation constants normalized with respect to the vacuum wavenumber  $k_0$ , viz.,  $\hat{\beta} = \beta/k_0$  and  $\hat{\alpha} = \alpha/k_0$ . As desired for the generation of an inward cylindrical leaky wave, needed for the excitation of a focused beam,<sup>39</sup> a negative value for  $\hat{\beta}$  and a positive value for  $\hat{\alpha}$  are achieved. Moreover, as expected, the dispersion curve of the TE leaky wave propagating in the structure lies within the curves of the fundamental TE modes for the limiting unperturbed cases of a parallel-plate waveguide (PPW) and a GDS. In addition, from the leaky phase and attenuation constants at the working frequency  $f_0 = 300$  GHz (viz.,  $\hat{\beta} = -0.461$  and  $\hat{\alpha} = 0.019$ ), one can determine the BB-launcher axicon angle  $\theta_0 = \arcsin(\hat{\beta}) \simeq 25^\circ$  and the radiation efficiency  $\eta_r = 1 - \exp(-2\rho_{ap}\hat{\alpha}) \simeq 95\%$ , with  $\rho_{ap} = 12.75$  mm being the radius of the launcher.<sup>40</sup> The axicon angle determines the nondiffractive range, i.e., the maximum distance for which a BB distribution approximately maintains its self-healing and diffraction-limited properties, through the ray-optics formula  $z_{ndr} = \rho_{ap} \cot \theta_0$ . Therefore, the nondiffractive range is here equal to  $z_{ndr} = 24.2$  mm, corresponding to about  $24.5\lambda_0$ .

It is worth pointing out that the metal is assumed to be a perfect electric conductor (PEC). This hypothesis can be justified by considering a standard photolithographic process for the realization of a 200-nm-thick aluminum-based grating [a reduction of the bulk conductivity for aluminum (Al) thin films is expected for thicknesses lower than 150 nm as discussed in Ref. 41]. At 300 GHz, the skin depth of Al is about 50 nm, thus a 200-nm-thick Al film can be characterized with its bulk conductivity value (viz., 37.7 MS/m)<sup>42</sup> that leads to an equivalent sheet resistance of  $R_s = 177$  m $\Omega$  (Ref. 42). The obtained  $R_s$  value, in the worst-case scenario of a PPW, leads to an attenuation constant related to Ohmic losses of about  $\hat{\alpha}_c = 0.0014$  (Ref. 42). The latter, along with an attenuation constant due to radiation losses equal

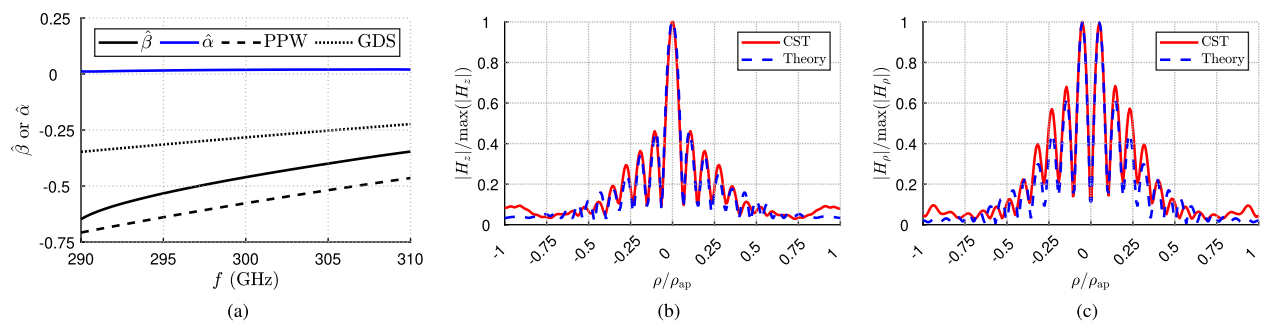


**FIG. 3.** (a) Dispersion curves of the leaky phase (black solid line) and attenuation (blue solid line) constants reported vs frequency  $f$  and normalized with respect to the vacuum wavenumber  $k_0$  (indicated by  $\hat{\beta} = \beta/k_0$ , and  $\hat{\alpha} = \alpha/k_0$ , respectively). The black dashed and dotted lines represent the unperturbed limit cases of a parallel-plate waveguide (PPW) and of a grounded dielectric slab (GDS) TE mode, respectively. Absolute value of the (b)  $H_z$  and (c)  $H_\rho$  components are reported, normalized with respect to their maximum on the  $z = z_{ndr}/2$  plane. The dashed blue line represents the theoretically predicted near-field distributions, while the red solid line shows the field obtained from a 3D full-wave simulation of the entire BB launcher.

to  $\hat{\alpha}_{\text{rad}} \simeq 0.019$  when  $|\hat{\beta}| = 0.46$  [see Fig. 3(a)], leads to a reduction of the overall antenna efficiency of about 5%—the radiation efficiency of a leaky structure, for  $|\beta| \gg \alpha$ , scales with the ratios of the attenuation constants between the lossless and lossy cases (see Refs. 43 and 44 for further details). This effect would be the only appreciable difference, since all the other near-field properties of the generated Bessel and Bessel–Gauss beams would practically remain the same. Therefore, metal losses are hereafter neglected and the metallic parts treated as PEC with considerable advantage in terms of computational burden in the full-wave simulations.

In order to corroborate the theoretical analysis, the entire 3D model of the device has been simulated using the time-domain solver of CST Microwave Studio. The considered design parameters, namely, the GDS height  $h = 0.38$  mm and dielectric permittivity  $\epsilon_r = 2.3(1 - j0.001)$  (representing a THz low-loss cyclo-olephin polymer<sup>30</sup>), the period of the metal strip grating  $p = 0.75$  mm, the slot width  $s = 0.33$  mm, the diameter of the central circular metallic patch  $D = 0.75$  mm, and the number of periods  $N = 16$ , are shown in Fig. 1. Full-wave results are reported through a red solid line in Figs. 3(b) and 3(c) for the vertical  $H_z$  and radial component  $H_\rho$ , respectively, of the magnetic field at  $z = z_{\text{ndr}}/2$ , normalized with respect to their maximum. As expected for a TE polarization,<sup>17</sup>  $H_z$  and  $H_\rho$  follow a  $J_0(\cdot)$  and a  $J_1(\cdot)$  radial distribution, respectively, where the BB is generated<sup>16</sup> (with  $J_q(\cdot)$  being the  $q$ th-order Bessel function of the first kind).

It is worth pointing out that simulated results are in a very good agreement with those obtained theoretically [blue dashed lines in Figs. 3(b) and 3(c)]. The latter are achieved by enforcing a dominant leaky-wave distribution given by an inward cylindrical leaky wave on the aperture plane.<sup>40</sup> In particular, for a TE-polarized BB launcher, being the dual case of the TM polarization,<sup>16</sup> the radial envelope of the non-vanishing tangential components is given by

$$E_\phi, H_\rho \propto H_1^{(2)}(k_\rho \rho), \quad (1)$$

with  $H_1^{(2)}(\cdot)$  being the Hankel function of the second kind and of the first order. With the leaky-wave aperture field at hand, one can predict the theoretical near-field distribution by exploiting the Huygens–Fresnel radiation integral<sup>29</sup> as in Ref. 40. In Fig. 3, the leaky-wave approach, the relevant design, and the dispersion diagram are validated by the excellent agreement between numerical [obtained through the

radiation integral of the field distribution in Eq. (1)] and full-wave results. It is worth pointing out that the *beam size*, commonly referred to as the null-to-null beam width (NNBW), can be theoretically computed as  $\text{NNBW} \simeq 4.81/\beta \simeq 1.7$  mm (Ref. 17) and this value is corroborated through full-wave simulations [see Fig. 3(b)].

Since BBs have a limited amount of power carried through their main lobe and show on-axis intensity oscillations due to edge diffraction,<sup>45</sup> the combination of BB and Gaussian-beam properties through leaky waves was proposed in Ref. 27, analyzing the nondiffracting features of BGBs. Starting from a leaky-wave design able to generate a BB distribution, it is possible to synthesize a BGB with a certain Gaussian-beam waist parameter  $w_0$  by properly tapering the radiating aperture. According to Ref. 27, in order to excite a TE-polarized BGB, one has to enforce the radially dependent normalized leaky attenuation constant,

$$\hat{\alpha}(\rho) = \frac{\lambda_0}{4\pi} \frac{\eta_r \rho |H_\rho^{\text{ap}}(\rho)|^2}{\int_0^{\rho_{\text{ap}}} \rho' |H_\rho^{\text{ap}}(\rho')|^2 d\rho' - \eta_r \int_0^{\rho} \rho' |H_\rho^{\text{ap}}(\rho')|^2 d\rho'} \quad (2)$$

with the radial magnetic-field component having the form

$$H_\rho^{\text{ap}}(\rho) = H_1^{(2)}(\beta \rho) e^{-(1/2)(\rho/w_0)^2}. \quad (3)$$

Therefore, from a practical viewpoint, one has to synthesize over the aperture plane the  $\hat{\alpha}$  value indicated by Eq. (2) while maintaining  $\hat{\beta}$  constant. This objective can be achieved by progressively changing the unit-cell design parameters. Since the phase constant mostly depends on  $p$  and the leakage constant can be significantly affected by variations of  $s$  (Ref. 16), the idea for a simple design procedure is to modify the slot width along the radius while maintaining the strip periodicity constant. As shown in Fig. 4(a) by the  $\hat{\beta}$  and  $\hat{\alpha}$  values computed for  $p = 0.75$  mm through the previously discussed Bloch analysis at  $f_0$ , the phase constant is almost flat for  $s < 0.41$  mm, while the leakage constant spans from 0 to  $\hat{\alpha}_{\text{max}} \simeq 0.025$ , with  $\hat{\alpha}_{\text{max}}$  being the maximum value that can be obtained for the selected value of  $p$ .

In order to verify the proposed approach, a case study is addressed below. Since the best range for the beam waist parameter normalized with respect to the aperture radius, viz.,  $\tilde{w}_0 = w_0/\rho_{\text{ap}}$ , is  $0.4 \leq \tilde{w}_0 \leq 0.6$  (Ref. 27),  $\tilde{w}_0 = 0.5$  is assumed in the following. In this case, by considering  $\beta = -0.41$  and  $\eta_r = 90\%$ , Eqs. (2) and (3)

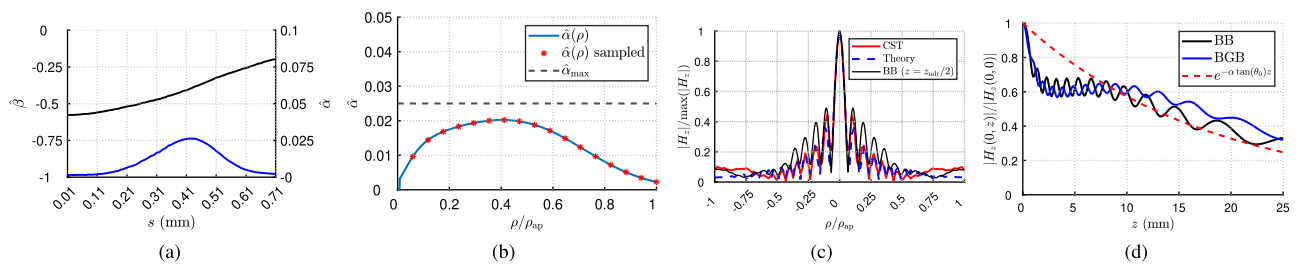


**FIG. 4.** (a) Normalized leaky phase (black solid line) and attenuation (blue solid line) constants at  $f_0$  for different slot-width values  $s$ . (b) Desired, continuous distribution of the normalized leaky attenuation constant (blue solid line) and its sampling (red asterisks) for the generation of a TE-polarized BGB with  $\tilde{w}_0 = 0.5$ . The black dashed line represents the maximum value that can be synthesized with the proposed unit-cell period and configuration. (c) Full-wave (red solid line) and theoretical (blue dashed line) evaluations of the  $H_z$  radial distribution on the  $z = z_{\text{ndr}}^{\text{BGB}}/2$  plane normalized with respect to its maximum for the proposed TE-polarized BGB launcher. The black solid line represents  $|H_z|(\rho, z = z_{\text{ndr}}/2)$  normalized with respect to its maximum for the BB launcher to show the higher concentration of power in the central lobes in the case of a BGB. (d) On-axis  $|H_z|$  1D profile (for  $\rho = 0$ ) vs  $z$  normalized with respect to its maximum for the TE-polarized BB (black solid line) and BGB (blue solid line) launcher. The red solid line represents the expected amplitude exponential decay for a leaky-wave BB or BGB launcher.<sup>40</sup>

generate the radial profile of  $\hat{\alpha}$  reported by the blue solid line in Fig. 4(b), which is always below  $\hat{\alpha}_{\max}$ ; this condition ensures in principle the exact leaky-wave synthesis of the desired beam. Therefore, by sampling the value of Eq. (2) for each period, the desired leakage constant is synthesized by adjusting  $s$  in each unit cell as reported in Table II. The running index of  $s$  represents the period number, which increases from the center toward the aperture radius. It is worth pointing out that the BGB nondiffractive range differs from that of the BB launcher since, for  $\tilde{w}_0 < 1/(\sqrt{\ln 4})$ , it is just a fraction of it. In particular, it reads as follows (Ref. 27):  $z_{\text{ndr}}^{\text{BGB}} = z_{\text{ndr}} \tilde{w}_0 \sqrt{\ln 4}$ , which corresponds to  $z_{\text{ndr}}^{\text{BGB}} \simeq 0.6z_{\text{ndr}} \simeq 14.5$  mm.

In order to corroborate the proposed analysis and achieve a realistic design of the proposed original TE-polarized BGB launcher, a 3D model of the device has been simulated using the time-domain solver of CST Microwave Studio. The structure is realized on a GDS with the same electric and geometrical features as the BB launcher. It consists of annular strips printed on the GDS with a period  $p = 0.75$  mm and whose widths are tapered as reported in Table II. The circular slot etched on the ground is fed by the CW output of the previously discussed Marié transducer. As shown in Fig. 4(c), full-wave results are in very good agreement with the theoretical ones, validating the leaky-wave design of the structure. It is worth noticing that a beam size of about 1.9 mm is achieved in this case, a value which is slightly larger than the BB distribution as expected due to the lower  $\hat{\beta}$  value considered for the BGB. The theoretical near-field distribution has been obtained by assuming a dominant leaky-wave contribution [i.e., using Eq. (3)] on the radiating aperture. The minimal differences among theoretical and full-wave results are justified by both the discretized physical implementation of Eq. (2) in the realistic scenario and by the smooth variation of  $\hat{\beta}$  along the aperture radius. It is worth pointing out that the main advantages of a BGB have been achieved also for TE polarization: the field intensity is concentrated on the central lobes whereas the amplitude level on the side lobes is significantly reduced, almost halved after the second null [see the difference between BB and BGB in Fig. 4(c)]. Moreover, the on-axis oscillations have been strongly reduced [see Fig. 4(d)]. In Fig. 4(d), the exponential decay profile of the amplitude of the  $|H_z|$  component is also evident, which can be described, in leaky-wave devices, through  $e^{-\alpha \tan(\theta_0)z}$ , as shown in Ref. 40.

In conclusion, in this work we have addressed the analysis and design of TE-polarized, (sub)millimeter-wave, leaky-wave beam launchers for the generation of focusing, diffraction-limited beams in the radiative near-field region. TE-polarized Bessel or Bessel–Gauss beams with a beam size of  $1.7\lambda_0$  and  $1.9\lambda_0$  have been obtained through a leaky-wave approach at 300 GHz up to a nondiffractive distance of  $24.5\lambda_0$  and  $14.5\lambda_0$ , respectively. Moreover, the implementation of a realistic, innovative feeder, matched through an effective

TABLE II. Width of the slots in millimeters for the proposed BGB launcher.

$s_1$	$s_2$	$s_3$	$s_4$	$s_5$	$s_6$	$s_7$	$s_8$
0.25	0.29	0.32	0.32	0.33	0.34	0.35	0.38
$s_9$	$s_{10}$	$s_{11}$	$s_{12}$	$s_{13}$	$s_{14}$	$s_{15}$	$s_{16}$
0.33	0.32	0.29	0.27	0.25	0.22	0.19	0.15

semi-analytical approach is presented. Demonstrated results pave the way for developing Bessel and Bessel–Gauss launchers also at submillimeter-wave frequencies, providing a robust, azimuthally symmetric, and realistic feeder for TE-polarized devices, which is currently lacking.

E.N. and W.F. acknowledge the project PRIN 2022 “SAFE” (Spiral and Focused Electromagnetic fields) 2022ESAC3K, Italian Ministry of University and Research (MUR), financed by the European Union, Next Generation EU. A.G. thanks for the support of the European Union under the Italian National Recovery and Resilience Plan (NRRP) of NextGenerationEU, partnership on “Telecommunications of the Future” (PE00000001—program “RESTART”).

## AUTHOR DECLARATIONS

### Conflict of Interest

The authors have no conflicts to disclose.

### Author Contributions

**E. Negri:** Conceptualization (equal); Data curation (equal); Formal analysis (equal); Investigation (equal); Methodology (equal); Software (equal); Validation (equal); Writing – original draft (equal); Writing – review & editing (equal). **W. Fuscaldo:** Conceptualization (equal); Data curation (equal); Formal analysis (equal); Funding acquisition (equal); Supervision (equal); Writing – original draft (equal); Writing – review & editing (equal). **D. González Ovejero:** Conceptualization (equal); Investigation (equal); Methodology (equal); Supervision (equal); Writing – review & editing (equal). **P. Burghignoli:** Conceptualization (equal); Formal analysis (equal); Methodology (equal); Writing – review & editing (equal). **A. Galli:** Conceptualization (equal); Formal analysis (equal); Funding acquisition (equal); Methodology (equal); Writing – review & editing (equal).

## DATA AVAILABILITY

The data that support the findings of this study are available from the corresponding author upon reasonable request.

## REFERENCES

- S. Chen, S. Li, Y. Zhao, J. Liu, L. Zhu, A. Wang, J. Du, L. Shen, and J. Wang, “Demonstration of 20-Gbit/s high-speed Bessel beam encoding/decoding link with adaptive turbulence compensation,” *Opt. Lett.* **41**, 4680–4683 (2016).
- E. Negri, W. Fuscaldo, P. Burghignoli, and A. Galli, “Leaky-wave analysis of TM-, TE-, and hybrid-polarized aperture-fed Bessel-beam launchers for wireless power transfer links,” *IEEE Trans. Antennas Propag.* **71**, 1424–1436 (2023).
- E. Negri, L. Del Biondo, W. Fuscaldo, P. Burghignoli, and A. Galli, “Wireless radiative near-field links through wideband Bessel-beam launchers,” in *53rd European Microwave Conference (EuMC 2023)*, Berlin, Germany (IEEE, 2023), pp. 1–4.
- C. Liu, Z. Zhao, C. Jin, Y. Xiao, G. Gao, H. Xie, Q. Dai, H. Yin, and L. Kong, “High-speed, multi-modal, label-free imaging of pathological slices with a Bessel beam,” *Biomed. Opt. Express* **11**, 2694–2704 (2020).
- T. A. Planchon, L. Gao, D. E. Milkie, M. W. Davidson, J. A. Galbraith, C. G. Galbraith, and E. Betzig, “Rapid three-dimensional isotropic imaging of living cells using Bessel beam plane illumination,” *Nat. Methods* **8**, 417–423 (2011).
- J. Durnin, J. J. Miceli, Jr., and J. H. Eberly, “Diffraction-free beams,” *Phys. Rev. Lett.* **58**, 1499 (1987).

- <sup>7</sup>D. McGloin and K. Dholakia, "Bessel beams: Diffraction in a new light," *Contemp. Phys.* **46**, 15–28 (2005).
- <sup>8</sup>Z. Li, K. B. Alici, H. Caglayan, and E. Ozbay, "Generation of an axially asymmetric Bessel-like beam from a metallic subwavelength aperture," *Phys. Rev. Lett.* **102**, 143901 (2009).
- <sup>9</sup>P. Lemaitre-Auger, S. Abielmona, and C. Caloz, "Generation of Bessel beams by two-dimensional antenna arrays using sub-sampled distributions," *IEEE Trans. Antennas Propag.* **61**, 1838–1849 (2013).
- <sup>10</sup>S. C. Pavone, M. Ettorre, and M. Albani, "Analysis and design of Bessel-beam launchers: Longitudinal polarization," *IEEE Trans. Antennas Propag.* **64**, 2311–2318 (2016).
- <sup>11</sup>M. Ettorre, S. C. Pavone, M. Casaletti, M. Albani, A. Mazzinghi, and A. Freni, "Near-field focusing by non-diffracting Bessel beams," in *Aperture Antennas for Millimeter and Sub-Millimeter Wave Applications* (Springer, Cham, Switzerland, 2018), pp. 243–288.
- <sup>12</sup>N. Chiotellis, S. Zhang, Y. C. Vardaxoglou, and A. Grbic, "X wave radiator implemented with 3D printed metamaterials," *IEEE Trans. Antennas Propag.* **68**, 5478–5486 (2020).
- <sup>13</sup>R. Cicchetti, A. Faraone, and O. Testa, "Energy-based representation of multi-port circuits and antennas suitable for near- and far-field syntheses," *IEEE Trans. Antennas Propag.* **67**, 85–98 (2019).
- <sup>14</sup>M. Ettorre and A. Grbic, "Generation of propagating Bessel beams using leaky-wave modes," *IEEE Trans. Antennas Propag.* **60**, 3605–3613 (2012).
- <sup>15</sup>W. Fuscaldo, G. Valerio, A. Galli, R. Sauleau, A. Grbic, and M. Ettorre, "Higher-order leaky-mode Bessel-beam launcher," *IEEE Trans. Antennas Propag.* **64**, 904–913 (2016).
- <sup>16</sup>D. Comite, W. Fuscaldo, S. K. Podilchak, P. D. Hilarío-Re, V. Gómez-Guillamón Buendía, P. Burghignoli, P. Baccarelli, and A. Galli, "Radially periodic leaky-wave antenna for Bessel beam generation over a wide-frequency range," *IEEE Trans. Antennas Propag.* **66**, 2828–2843 (2018).
- <sup>17</sup>E. Negri, W. Fuscaldo, P. Burghignoli, and A. Galli, "A leaky-wave analysis of resonant Bessel-beam launchers: Design criteria, practical examples, and potential applications at microwave and millimeter-wave frequencies," *Micromachines* **13**, 2230 (2022a).
- <sup>18</sup>C. Tumbaga, "Modernizing mm-wave measurements with 110 GHz coaxial components," *Microwave J.* **63**, 98–102 (2020).
- <sup>19</sup>P. Lu, D. Voyer, A. Bréard, J. Huillery, B. Allard, X. Lin-Shi, and X.-S. Yang, "Design of TE-polarized Bessel antenna in microwave range using leaky-wave modes," *IEEE Trans. Antennas Propag.* **66**, 32–41 (2018).
- <sup>20</sup>E. Negri, F. Benassi, W. Fuscaldo, D. Masotti, P. Burghignoli, A. Costanzo, and A. Galli, "Design of TE-polarized resonant Bessel-beam launchers for wireless power transfer links in the radiative near-field region," *Int. J. Microwave Wireless Technol.* (available online 2024).
- <sup>21</sup>P. Lu, A. Bréard, J. Huillery, X.-S. Yang, and D. Voyer, "Feeding coils design for TE-polarized Bessel antenna to generate rotationally symmetric magnetic field distribution," *Antennas Wireless Propag. Lett.* **17**, 2424–2428 (2018).
- <sup>22</sup>F. Benassi, E. Negri, W. Fuscaldo, G. Paolini, F. Maita, P. Burghignoli, D. Masotti, A. Galli, and A. Costanzo, "TE-polarized Bessel-beam launchers for wireless power transfer at millimeter waves: Theory, design, and experimental validation," *IEEE Trans. Microwave Theory Tech.* (available online 2024).
- <sup>23</sup>E. S. Gámez Rodríguez, M. Machnoor, and G. Lazzi, "On the generation of nondiffracting beams in extremely subwavelength applications," *IEEE Trans. Antennas Propag.* **65**, 5228–5237 (2017).
- <sup>24</sup>E. Negri, W. Fuscaldo, S. Tofani, P. Burghignoli, and A. Galli, "An efficient and accurate semi-analytical matching technique for waveguide-fed antennas," *Sci. Rep.* **14**, 3892 (2024).
- <sup>25</sup>K. Matheson, K. Ronald, D. Speirs, A. Phelps, and A. Cross, "An X-band rectangular TE<sub>10</sub> to circular TE<sub>01</sub> Mode converter," in *2nd Annual Passive RF and Microwave Components Seminar* (IET, Glasgow, UK, 2011).
- <sup>26</sup>S. Saad, J. Davies, and O. Davies, "Analysis and design of a circular TE<sub>01</sub> mode transducer," *IEEE J. Microwave Opt. Acoust. UK.* **1**, 58–62 (1977).
- <sup>27</sup>W. Fuscaldo, A. Benedetti, D. Comite, P. Baccarelli, P. Burghignoli, and A. Galli, "Bessel-Gauss beams through leaky waves: Focusing and diffractive properties," *Phys. Rev. Appl.* **13**, 064040 (2020).
- <sup>28</sup>E. Negri, F. Benassi, W. Fuscaldo, D. Masotti, P. Burghignoli, A. Costanzo, and A. Galli, "Effective TE-polarized Bessel-beam excitation for wireless power transfer near-field links," in *52nd European Microwave Conference (EuMC 2022)*, Milan, IT (IEEE, 2022), pp. 1–4.
- <sup>29</sup>C. A. Balanis, *Advanced Engineering Electromagnetics* (Wiley & Sons, New York, NY, 2012).
- <sup>30</sup>W. Fuscaldo, S. Tofani, D. C. Zografopoulos, P. Baccarelli, P. Burghignoli, R. Beccherelli, and A. Galli, "Systematic design of THz leaky-wave antennas based on homogenized metasurfaces," *IEEE Trans. Antennas Propag.* **66**, 1169–1178 (2018).
- <sup>31</sup>M. Del Mastro, M. A. Del Pino, and M. Spirito, "A 3D printed TE<sub>10</sub> rectangular to TE<sub>01</sub> circular waveguide transition for polymer waveguide characterization," in *92nd ARFTG Microwave Measurement Conference (ARFTG)*, Orlando, FL (IEEE, 2019), pp. 1–3.
- <sup>32</sup>M. Ettorre and D. G. Ovejero, "High speed and resilient wireless interconnects in the near field," in *International Workshop on Antenna Technology (iWAT)*, Aalborg, Denmark (IEEE, 2023), pp. 1–4.
- <sup>33</sup>C. Lee, D. Gonzalez-Ovejero, M. Alonso-delPino, T. Reck, A. Peralta, I. Mehdi, and G. Chattopadhyay, "Corrugated (2 × 2) silicon platelets horn antenna array at 560 GHz," in *42nd International Conference Infrared, Millimeter, and Terahertz Waves (IRMMW-THz)*, Cancun, Mexico (IEEE, 2017), p. 1.
- <sup>34</sup>R. E. Collin, *Field Theory of Guided Waves* (John Wiley & Sons, New York, NY, 1990).
- <sup>35</sup>P. Baccarelli, P. Burghignoli, C. Di Nallo, F. Frezza, A. Galli, P. Lampariello, and G. Ruggieri, "Full-wave analysis of printed leaky-wave phased arrays," *Int. J. RF Microwave Comput. Aided Eng.* **12**, 272–287 (2002).
- <sup>36</sup>G. Valerio, S. Paulotto, P. Baccarelli, P. Burghignoli, and A. Galli, "Accurate Bloch analysis of 1-D periodic lines through the simulation of truncated structures," *IEEE Trans. Antennas Propag.* **59**, 2188–2195 (2011).
- <sup>37</sup>F. Giusti, Q. Chen, F. Mesa, M. Albani, and O. Quevedo-Teruel, "Efficient Bloch analysis of general periodic structures with a linearized multimodal transfer-matrix approach," *IEEE Trans. Antennas Propag.* **70**, 5555–5562 (2022).
- <sup>38</sup>N. Apaydin, L. Zhang, K. Sertel, and J. L. Volakis, "Experimental validation of frozen modes guided on printed coupled transmission lines," *IEEE Trans. Microwave Theory Tech.* **60**, 1513–1519 (2012).
- <sup>39</sup>M. Albani, S. C. Pavone, M. Casaletti, and M. Ettorre, "Generation of non-diffractive Bessel beams by inward cylindrical traveling wave aperture distributions," *Opt. Express* **22**, 18354–18364 (2014).
- <sup>40</sup>W. Fuscaldo, D. Comite, A. Boesso, P. Baccarelli, P. Burghignoli, and A. Galli, "Focusing leaky waves: A class of electromagnetic localized waves with complex spectra," *Phys. Rev. Appl.* **9**, 054005 (2018).
- <sup>41</sup>N. Laman and D. Grischkowsky, "Terahertz conductivity of thin metal films," *Appl. Phys. Lett.* **93**, 051105 (2008).
- <sup>42</sup>D. M. Pozar, *Microwave Engineering: Theory and Techniques* (John Wiley & Sons, 2021).
- <sup>43</sup>W. Fuscaldo, "Rigorous evaluation of losses in uniform leaky-wave antennas," *IEEE Trans. Antennas Propag.* **68**, 643–655 (2020).
- <sup>44</sup>C. Di Nallo, F. Frezza, A. Galli, and P. Lampariello, "Rigorous evaluation of Ohmic-loss effects for accurate design of traveling-wave antennas," *J. Electromagn. Waves Appl.* **12**, 39–58 (1998).
- <sup>45</sup>W. Fuscaldo, P. Burghignoli, and A. Galli, "A comparative analysis of Bessel and Gaussian beams beyond the paraxial approximation," *Optik* **240**, 166834 (2021).